symmetry

IMPACT FACTOR 2.2

CITESCORE 5.3

Article

# Quantum Fisher Information Probing a Quantum-Gas Cavity QED

Lehan Zhu, Qian Wang and Zhaoxin Liang

Special Issue

Symmetry Methods and Applications in Quantum Optics and Quantum Information

Edited by

Dr. Mohamed Amazioug and Prof. Dr. Mohammed Daoud

MDPI

https://doi.org/10.3390/sym17111918

symmetry

MDPI

*Article*

# Quantum Fisher Information Probing a Quantum-Gas Cavity QED

**Lehan Zhu [1], Qian Wang [2] and Zhaoxin Liang [2,*]**

[1] Department of Physics, Fudan University, Shanghai 200438, China; 23210190058@m.fudan.edu.cn
[2] Department of Physics, Zhejiang Normal University, Jinhua 321004, China
* Correspondence: zhxliang@zjnu.edu.cn

**Abstract**

Motivated by recent efforts in simulating nonequilibrium scenarios of the Dicke model in quantum-gas cavity QED, we investigate direct probing of the normal-to-superradiant quantum phase transition via Quantum Fisher Information (QFI). This transition represents a paradigmatic example of spontaneous symmetry breaking in quantum optics, where the system's $Z_2$ symmetry is broken in the superradiant phase. At zero temperature, we derive analytical expressions for the QFI in the limit where the atomic transition frequency—scaled by the cavity frequency—tends to infinity. Furthermore, we analyze the impact of finite temperature on the QFI in both the thermodynamic limit and the regime of a finite but large number of atoms. All results demonstrate that the QFI exhibits a singularity as the coupling crosses the critical point—a clear signature of quantum criticality associated with spontaneous symmetry breaking. The divergent behavior of the QFI across the quantum phase transition directly relates to measuring dynamic susceptibilities using experimentally accessible Bragg spectroscopy tools and resources.

**Keywords:** Dicke model; Quantum Fisher Information; quantum phase transition; superradiant phase; Bragg spectroscopy; symmetry breaking



Academic Editors: Mohamed Amazioug and Mohammed Daoud

Received: 2 October 2025
Revised: 2 November 2025
Accepted: 6 November 2025
Published: 9 November 2025

**Citation:** Zhu, L.; Wang, Q.; Liang, Z. Quantum Fisher Information Probing a Quantum-Gas Cavity QED. *Symmetry* **2025**, *17*, 1918. https://doi.org/10.3390/sym17111918



## 1. Introduction

Light–matter interactions are the cornerstone of quantum information processing and quantum state engineering—a theme underscored in numerous reviews [1–4]. Quantum-gas cavity QED (cavity-QED) [5,6] now leads the way in unraveling and controlling such interactions. The revival of this field is largely attributed to pivotal theoretical breakthroughs, such as Braak's seminal work on the integrability of the quantum Rabi model, which ignited intense research into fundamental light–matter models and their extensions [7]. Unlike conventional quantum optics, cavity-QED is defined by two defining features [5,6]: repeated light-atom coupling to the same atomic ensemble, and the backaction of atoms on the light field—both of which govern the collective dynamics. Consequently, cavity-QED hosts exotic nonclassical phenomena—making it an ideal platform for quantum metrology [8,9]. Moreover, its nondestructive probing via cavity leakage photons positions cavity-QED as a unique system for exploring nonequilibrium many-body phases, yielding insights inaccessible in traditional condensed-matter physics [10].

Within this research thread, simulating nonequilibrium Dicke model scenarios in cavity-QED has emerged as a focal topic [5,6]. The Dicke model exhibits a rich symmetry structure, with a normal phase preserving the $Z_2$ symmetry and a superradiant phase where this symmetry is spontaneously broken. A landmark theoretical proposal [11] put forward realizing an open Dicke model via cavity-assisted Raman transitions, aiming to

characterize the associated superradiant phase transition. Building on this concept [11], experiments with Bose–Einstein condensates (BECs) coupled to high-finesse cavities linked self-organization to the Dicke model—and culminated in the groundbreaking observation of the phase transition by Baumann et al. [12], which marked a pivotal experimental milestone. Yet, directly measuring quantum phases across the critical point in experiments remains a persistent challenge.

Theoretical efforts have long recognized that metrics from quantum information theory provide a powerful means to probe such criticality. For instance, Ashhab's study of the quantum Rabi model demonstrated that the sharp increase in the entanglement entropy and the peak of squeezing at the critical point serve as clear signatures of the quantum phase transition [13], establishing entanglement entropy as a sensitive probe. Theoretical works [14–17] proposed using entanglement as a quantifier for quantum phase transitions, via density matrix tomography. For few-atom optical lattices, protocols leveraging atomic physics tools—single-site manipulation and readout—measure entanglement entropy and state purity by replicating the quantum system. However, a key limitation is their exponential resource scaling, which restricts these approaches to small system sizes.

In this work, we propose a method to characterize the Dicke model's quantum phase transition (QPT) in cavity-QED—specifically across the critical point—using experimentally accessible tools. Our approach leverages the Quantum Fisher Information (QFI), which, akin to entanglement entropy, is an information-theoretic measure but offers a more direct characterization of symmetry breaking and critical fluctuations, a quantity directly connectable to dynamic susceptibility measurements via Bragg spectroscopy (a technique with experimental reach). Importantly, the QFI serves as a sensitive probe of symmetry-breaking phenomena, as it captures the system's sensitivity to parameter variations near critical points where symmetries are spontaneously broken. At zero temperature, we derive analytical QFI expressions in the limit where the atomic transition frequency (scaled by the cavity frequency) tends to infinity. We additionally analyze finite-temperature QFI effects in both the thermodynamic limit and for large but finite atom numbers. All results show a singularity in the QFI as coupling increases across the critical point—a distinct signature of quantum criticality. This divergent QFI behavior during the phase transition directly relates to measuring dynamic susceptibilities with Bragg spectroscopy, bridging theoretical predictions to experimental practice.

This paper is structured as follows. In Section 2, we introduce the model system—where the self-organization phase transition corresponds to a subradiant quantum phase transition involving spontaneous symmetry breaking. In Section 3, we show how the QFI serves as an efficient probe for dynamic Dicke superradiance in a BEC coupled to an optical cavity. Finally, in Section 4, we discuss experimental accessibility of the described phenomena and conclude with a summary of our work.

## 2. Model Hamiltonian and Quantum Fisher Information

We study a BEC of $N$ atoms (mass $m$) confined in a cavity of length $L$ [12,18–22]. Their internal motion couples to a cavity mode (operator $\hat{a}$, frequency $\omega_C$). We describe the bosonic matter-wave field ($\hat{\psi}(x)$) using a two-mode momentum expansion [14]: specifically, $\hat{\psi}(x) = (\hat{c}_0 + \sqrt{2}\hat{c}_1 \cos kx)/\sqrt{L}$. Using the Schwinger representation, we define spin components: $\hat{S}_x = \frac{1}{2}(\hat{c}_1^\dagger \hat{c}_0 + \hat{c}_0^\dagger \hat{c}_1)$ and $\hat{S}_z = \frac{1}{2}(\hat{c}_1^\dagger \hat{c}_1 - \hat{c}_0^\dagger \hat{c}_0)$. The resulting effective Hamiltonian maps to a Dicke-like model, as detailed in Ref. [14] and derived in Appendix A:

$$H = \omega_R \hat{S}_z - \delta_c \hat{a}^\dagger \hat{a} + \frac{iy}{\sqrt{N}}(\hat{a}^\dagger - \hat{a})\hat{S}_x + \frac{u}{2}\hat{a}^\dagger \hat{a}\left(1 + \frac{2\hat{S}_z}{N}\right), \tag{1}$$

In this Hamiltonian (1), $\hat{S}_x, \hat{S}_z$ are the Pauli matrices for the two-mode bosonic field (Schwinger representation), and $\hat{a}$ ($\hat{a}^\dagger$) denotes the cavity annihilation (creation) operator. The recoil frequency is $\omega_R = \hbar k^2/(2m)$. The tunable detuning $\delta_c = \Delta_C - 2u$ combines the effective photon energy in the cavity $\Delta_C = \omega - \omega_C$, which we tune via the pump laser frequency $\omega$. The coupling strength $y = \sqrt{2N}\eta_t$ is controlled by the transverse driving amplitude $\eta_t = \Omega g_0/\Delta_A$—here, $\Omega$ is the transverse driving Rabi frequency, $g_0$ the single-photon Rabi frequency at the cavity antinode, and $\Delta_A = \omega - \omega_A$ the atom-pump detuning ($\omega_A$ = atomic resonance frequency). Note that the last term in Equation (1) is small ($u = NU_0/4$) and often negligible in cavity QED. We remark that the parity operator, which measures an even-odd parity of total excitation number and reads $\Pi = \exp(i\pi[\hat{a}^\dagger\hat{a} + \frac{1}{2}(1 + 2S_z/N)])$, commutes with Hamiltonian (1). Therefore, Hamiltonian (1) has the $Z_2$ parity symmetry [23].

The Dicke-like Hamiltonian (Equation (1)) describes the interplay between $N$ two-level atoms and a single bosonic mode, building on Dicke's seminal work [24]. This model is known to host a quantum phase transition (QPT) from the normal to superradiant phase as atom-field coupling strengthens [14,25,26]. Specifically, for coupling strength $y \leq y_c = \sqrt{-\omega_R\delta_c}$, the system remains in the normal phase; for $y > y_c$, it transitions to the superradiant phase.

Here, we use Quantum Fisher Information (QFI) to characterize this normal-to-superradiant QPT in Equation (1) Hamiltonian—a direct probe for symmetry-breaking phenomena. The QFI, denoted as $F_I$, quantifies the distinguishability between a density matrix $\rho$ and its unitary transform $\rho' = e^{-i\theta\hat{O}}\rho e^{i\theta\hat{O}}$—induced by a Hermitian operator $\hat{O}$ with small phase $\theta$. For a pure state $\rho = |\psi(\theta)\rangle\langle\psi(\theta)|$, QFI is given by [27–32]:

$$F_I = 4\Big[\langle\partial_\theta\psi(\theta)|\partial_\theta\psi(\theta)\rangle - |\langle\psi(\theta)|\partial_\theta\psi(\theta)\rangle|^2\Big]. \tag{2}$$

For a mixed state in thermal equilibrium, the QFI is expressed as [27–32]:

$$F_I = 2\sum_{n,n'}\frac{(p_n - p_{n'})^2}{p_n + p_{n'}}|\langle n|\hat{O}|n'\rangle|^2, \tag{3}$$

where $p_n = \exp(-E_n/k_BT)/Z$ represents the occupation probability in the energy eigenbasis $|n\rangle$, with $Z = \sum_n \exp(-E_n/k_BT)$ being the partition function.

The key idea behind the utility of QFI to detect the quantum phase transition can be explained as follows: when one adiabatically drives the system across the critical point, a divergent Fisher information is expected to occur [33,34]. This effectiveness stems from the closing of the energy gap above the ground state during continuous quantum phase transitions in the thermodynamic limit. Consider the ground state $|\psi_0\rangle$ of a Hamiltonian $\hat{H}(y) = \sum_0 E_n(y)|\psi_n(y)\rangle\langle\psi_n(y)|$. The impact of a vanishing energy gap on the Quantum Fisher Information, as given by Equation (2), becomes evident from the expression:

$$F_I = 4\sum_{n\neq 0}\frac{\left|\langle\psi_n(y)\left|\partial_y\hat{H}(y)\right|\psi_n(y)\rangle\right|^2}{[E_n(y) - E_0(y)]^2}. \tag{4}$$

Clearly, as the energy gap above the ground state narrows in the denominator, the Quantum Fisher Information soars. This property potentially enables arbitrarily high precision in measuring phase transitions in the thermodynamic limit. In the subsequent sections, we will explore the quantum phase transitions of the Hamiltonian described by Equation (1) by calculating the QFI using Equations (2) and (3).

It is worth noting that while Ref. [33] also employed QFI as an indicator of the superradiant quantum phase transition, our current work differs in several key aspects:

(i) The light–matter coupling inherent in our practical experimental setup is complex, whereas the one examined in Ref. [33] is real. This necessitates a distinct approach to analyzing the Hamiltonian at finite temperatures, as reflected in Equation (12). (ii) We obtain analytical expressions for the QFI at zero temperature, rather than relying solely on numerical solutions, which were not provided in Ref. [33]. Thus, our study, in conjunction with Ref. [33], offers a comprehensive framework for using the QFI to probe the symmetry-breaking quantum phase transition of the Dicke-like Hamiltonian. We remark that Ref. [34] has demonstrated the feasibility of enhanced measurement by utilizing the critical divergent feature of QFI without the specific initial state preparation based on a cavity optomechanical Hamiltonian different from Hamiltonian (1).

## 3. Probing Quantum Phase Transition of Hamiltonian (1) via QFI

### *3.1. QFI at Zero Temperature*

In this section, we utilize the Quantum Fisher Information (QFI) given in Equation (2) to explore the quantum phase transition occurring at zero temperature, specifically within the limit where $|\delta_c|/(\omega_R N) \ll 1$. For clarity, let us denote the eigenstates of $S_z$ as $|\uparrow(\downarrow)\rangle$ and the eigenstates of $a^\dagger a$ as $|n\rangle$.

To commence our investigation, we calculate the QFI linked to the normal phase of the Hamiltonian (1) in the range of $y \leq y_c$. We employ a strategy that involves seeking a unitary Schrieffer–Wolff transformation [35]. This transformation, given by $\hat{U} = \exp\left[\frac{y}{(\omega_R\sqrt{N})}(a - a^\dagger)\hat{S}_y\right]$, decouples the two spin subspaces (namely, $H_\uparrow$ and $H_\downarrow$) in the transformed Hamiltonian $U^\dagger H U$. As a result, we derive the effective low-energy form of the Hamiltonian (1) in its normal phase as detailed in Appendix B:

$$\begin{aligned} H_{\rm np} &= \langle\downarrow|U^\dagger H U|\downarrow\rangle \\ &= -\delta_c \hat{a}^\dagger a + \frac{y^2}{4\omega_R}(\hat{a}^\dagger - \hat{a})^2 - \frac{N\omega_R}{2}. \end{aligned} \tag{5}$$

The eigenvalues $E_{\rm np}$ and eigenstates $|\psi^n_{\rm nf}\rangle$ of this effective Hamiltonian $H_{\rm np}$ can be determined analytically. The eigenvalues of the Hamiltonian (5) are given by:

$$E_{\rm np} = -\delta_c\sqrt{1 - \left(\frac{y}{y_c}\right)^2}\left(n + \frac{1}{2}\right) + \frac{\delta_c}{2} + \frac{y^2}{4\omega_R}, \tag{6}$$

where $n = 0, 1, 2, \ldots$. The corresponding eigenstates, related to Equation (6), can be represented as $|\psi^n_{\rm np}\rangle = \hat{S}(\xi)|n\rangle \otimes |\downarrow\rangle$. Here, $\hat{S}(\xi) = \exp[\xi(a^{\dagger 2} - a^2)/2]$ is the squeezing operator, with $\xi = (1/4)\ln\left[1 - (y/y_c)^2\right]$ as the squeezing parameter.

Note that the eigenvalues $E_{\rm np}$ in Equation (6) are real only when the atom-field coupling $y$ is less than or equal to the critical value $y_c$, and they vanish precisely at this critical point. For the parameter range where $y \leq y_c$, we can substitute the derived $E_{\rm np}$ and the corresponding eigenstates $|\psi^n_{\rm nf}\rangle$ into Equation (2). This allows us to obtain the analytical expression for Quantum Fisher Information (QFI), given by:

$$\begin{aligned} F_{\rm I}^{\rm np} &= 4\left[\langle\partial_{\delta_c}\psi \mid \partial_{\delta_c}\psi\rangle - |\langle\partial_{\delta_c}\psi \mid \psi\rangle|^2\right] \\ &= \frac{(n^2 + n + 1)y^4}{8\delta_c^2(y_c + y)^2} \times \frac{1}{(y_c - y)^2}. \end{aligned} \tag{7}$$

From Equation (7), it is evident that QFI diverges as $y$ approaches $y_c$, indicating a quantum phase transition. Importantly, Equation (2) is not applicable for $y > y_c$.

Moving on, we explore the QFI associated with the superradiant phase of the model Hamiltonian (1) for $y > y_c$. In this phase, the number of photons within the cavity field be-

comes proportional to $N$. To capture the essential low-energy physics, we apply a similarity transformation $U^\dagger \hat{D}^\dagger(\alpha) H U \hat{D}(\alpha)$ to the Hamiltonian (1). Here, $\hat{D}(\alpha) = \exp[\alpha a^\dagger - \alpha^* a]$ is the displacement operator, and $U = e^{-i2\sigma_y \theta}$ represents a rotation transformation [14,35]. By choosing $\alpha^* - \alpha = -i\beta$ and $\tan(2\theta) = y\beta/(\omega_R\sqrt{N})$, we obtain the effective low-energy form of the Hamiltonian (1) in the superradiant phase as detailed in Appendix C

$$\begin{aligned} H_{\rm sp} &= U^\dagger \hat{D}^\dagger(\alpha) H \hat{D}(\alpha) U \\ &= -\delta_c \hat{a}^\dagger \hat{a} + \tilde{\omega}_R S_z + \frac{i\tilde{y}}{\sqrt{N}}\left(\hat{a}^\dagger - \hat{a}\right) S_x - \delta_c |\alpha|^2, \end{aligned} \tag{8}$$

where $\alpha = \pm i\sqrt{N\omega_R/(-4\delta_c)[(y/y_c)^2 - (y/y_c)^{-2}]}$, $\tilde{\omega}_R = \sqrt{\omega_R^2 - 4y^2\alpha^2/N}$, and $\tilde{y} = y\omega_R\sqrt{N}/\sqrt{\omega_R^2 N - 4y^2\alpha^2}$. Equation (8) bears structural similarity to the original Hamiltonian (1), but with rescaled parameters $\tilde{\omega}_R$ and $\tilde{y}$. This allows us to routinely derive the eigenstates of Equation (8) as $|\psi_{\rm sp}^n\rangle = \hat{S}(\xi)|n\rangle \otimes |\downarrow\rangle$, with $\xi = \frac{1}{4}\ln\left(1 + \frac{\tilde{y}^2}{\tilde{\omega}_R \delta_c}\right)$. The corresponding eigenvalue is given by:

$$\begin{aligned} E_{\rm sp} &= -\delta_c\sqrt{1 + \frac{\tilde{y}^2}{\tilde{\omega}_R\delta_c}}(n + \frac{1}{2}) + \frac{\delta_c}{2} + \frac{\tilde{y}^2}{4\tilde{\omega}_R} - \delta_c|\alpha|^2 \\ &= -\delta_c\sqrt{\left(1 + \frac{y_c^2}{y^2}\right)\left(1 - \frac{y_c^2}{y^2}\right)}\left(n + \frac{1}{2}\right) + \frac{\delta_c}{2} - \frac{\delta_c y_c^2}{4y} - \delta_c|\alpha|^2. \end{aligned} \tag{9}$$

For the standard parameters where $N > 0$, $\delta_c < 0$, and $\omega_R > 0$, the eigenvalue expressed in Equation (9) corresponds to that of the Hamiltonian (8) in the superradiant phase. This eigenvalue is real only if $y$ surpasses the critical value $y_c = \sqrt{-\delta_c \omega_R}$. Based on Equation (2), we can derive the analytical expression for Quantum Fisher Information (QFI) in the super-radiant phase as follows:

$$\begin{aligned} F_{\rm I}^{\rm sp} &= 4\Big(\langle \partial_{\delta_c}\psi \mid \partial_{\delta_c}\psi\rangle - |\langle \partial_{\delta_c}\psi \mid \psi\rangle|^2\Big) \\ &= \frac{(n^2 + n + 1)y_c^8}{8\delta_c^2(y^2 + y_c^2)^2(y + y_c)^2} \times \frac{1}{(y - y_c)^2}. \end{aligned} \tag{10}$$

It is worth noting that in the regime where $|\delta_c|/(\omega_R N) \ll 1$, the advanced corrections in Equations (5) and (8) become negligible [35]. Consequently, $H_{\rm np}$ from Equation (5) and $H_{\rm sp}$ from Equation (8) emerge as the precise low-energy effective Hamiltonians for the normal phase ($y < y_c$) and the superradiant phase ($y > y_c$), respectively. This implies that Equations (7) and (10) precisely represent the QFI of the Hamiltonian (1) in its respective phases.

Leveraging Equations (7) and (10), we can devise a method to detect the quantum phase transition inherent in the Hamiltonian (1). Let us explore some pivotal characteristics of this transition and its relationship to QFI as defined in Equation (2). Firstly, the rescaled cavity photon count, denoted as $n_c = |\delta_c|/\omega_R\langle \hat{a}^\dagger \hat{a}\rangle$, serves as an order parameter. It remains zero when $y < y_c$ and becomes finite, with a value of $(y^4 - y_c^4)/4y$, when $y > y_c$. Secondly, the rescaled ground state energy, computed as $\lim_{y\to y_c} E_{\rm np} = \delta/4 = \lim_{y\to y_c} E_{\rm sp}$, demonstrates continuity at the critical point $y = y_c$. However, a discontinuity arises in its second derivative, highlighting the second-order nature of the quantum phase transition. Thirdly, as we approach the critical point, the excitation energies in both phases vanish, proportional to $|1 - y^2/y_c^2|^{1/2}$ and $|1 - y_c^2/y^2|^{1/2}$ as indicated by Equations (6) and (9). Consequently, the QFI (2) diverges in a manner proportional to $|y - y_c|^{-2}$, aligning with the findings of Equations (7) and (10). This divergence is a hallmark of critical behavior

associated with symmetry breaking, where the system's response to external perturbations becomes singular. In Figure 1a,b, we illustrate the outcomes for QFI and its first derivative based on Equations (7) and (10). The red solid curves prominently showcase the divergence of QFI at the critical point $y = y_c$, a direct consequence of the narrowing energy gap above the ground state as expressed in Equation (4). In contrast, both QFI and its first derivative rapidly diminish to zero when $y$ moves away from $y_0$. This trend can be understood through Equation (2). When the system is not in the vicinity of the quantum phase transition's critical point, it becomes highly resistant to external perturbations represented by $\theta$. As a result, $\langle\psi(\theta)|\partial_\theta\psi(\theta)\rangle$ approaches unity, indicating a negligible QFI according to Equation (2). Finally, it is worth mentioning that the QFI depicted in Figure 1a and its first derivative in Figure 1b can be empirically determined by analyzing the squared Hellinger distance between probability distributions, as outlined in Ref. [32].

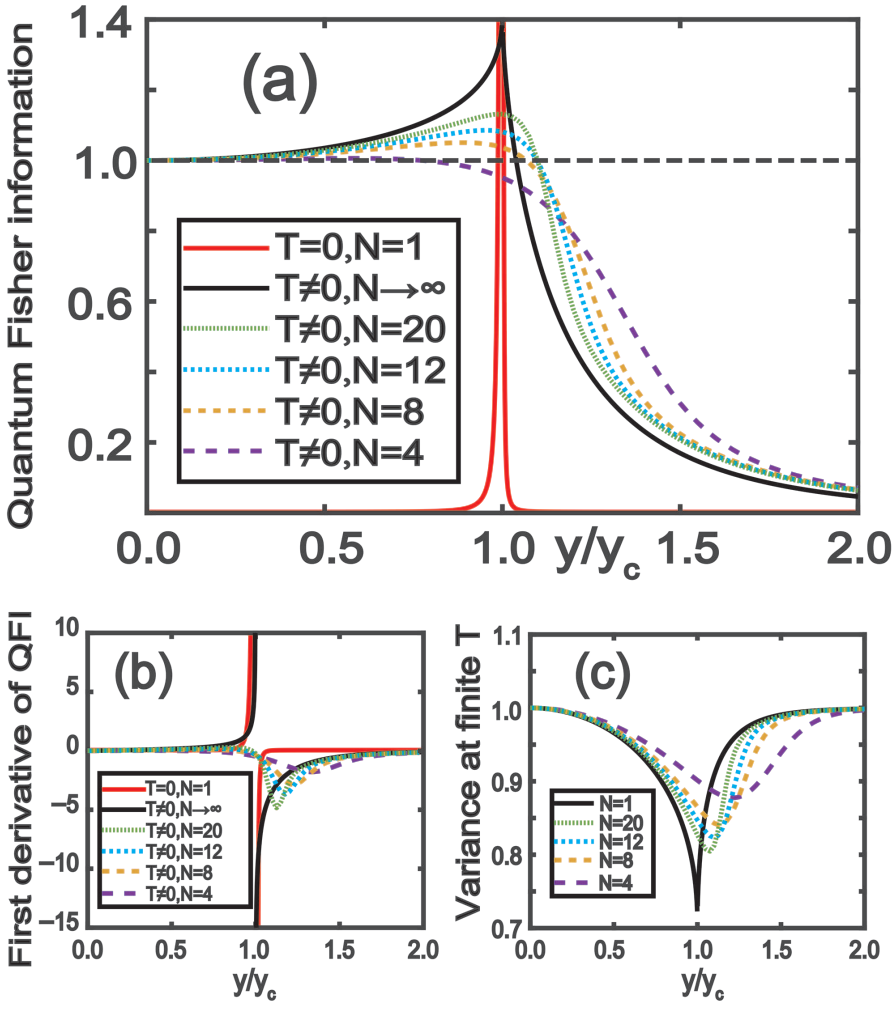


**Figure 1.** (**a**) Scaled Quantum Fisher Information plotted against the coupling coefficient $y$. (**b**) The scaled Quantum Fisher Information's first derivative graphed as a function of the coupling coefficient $y$. (**c**) Illustration of the spin squeezing parameter $\xi^2$ for the atoms versus the coupling strength $y$. Solid lines represent the analytical results of the QFI obtained in the thermodynamic limit, while dashed lines depict numerical outcomes for a finite number of atoms, specifically $N = 4$, 8, 12, and 20. The parameters used are $\delta_c = -1\omega_R$ and $u = -0.1\omega_R$.

### *3.2. The QFI at Finite Temperatures*

In Section 3.1, we analytically derived the QFI for the Hamiltonian (1) at zero temperature, as seen in Equations (7) and (10). Now, in this Section 3.2, our intention is to explore the influence of finite temperature on the QFI, utilizing Equation (3), particularly in the

thermodynamic limit where $N$ and $V$ tend to infinity while maintaining a constant atom density $N/V$.

Drawing from the work presented in Ref. [14], we adopt the Holstein–Primakoff transformation, specifically, $\hat{J}_+ = \hat{J}_-^\dagger = \hat{b}^\dagger\sqrt{N-\hat{b}^\dagger\hat{b}}$ and $\hat{J}_z = \hat{b}^\dagger\hat{b} - N/2$, to recast the atomic freedoms in terms of the bosonic operator $\hat{b}$. Through this lens, the Hamiltonian (1) can be reframed as:

$$\begin{aligned} H &= -\delta_c a^\dagger a + \omega_R b^\dagger b + u b^\dagger b a^\dagger a/N - N\omega_R/2 \\ &+ \frac{i}{2}y\left(a^\dagger - a\right)\left(b^\dagger\sqrt{1-\frac{b^\dagger b}{N}} + \sqrt{1-\frac{b^\dagger b}{N}}b\right). \end{aligned} \tag{11}$$

This reformulated Hamiltonian (11) elegantly describes the dynamics between two intertwined harmonic oscillators, denoted by the operators $\hat{a}$ and $\hat{b}$, respectively.

Shifting our focus to the system's normal phase, we introduce the position and momentum operators defined as $X_{1,2} = \left(a_{1,2}^\dagger + a_{1,2}\right)/\sqrt{2\omega_{1,2}}$ and $P_{1,2} = i\sqrt{\omega_{1,2}/2}\left(a_{1,2}^\dagger - a_{1,2}\right)$. Through this lens, Hamiltonian (11) transforms into:

$$H_{\rm np} = \frac{1}{2}(\omega_1^2 X_1^2 + P_1^2 + \omega_2^2 X_2^2 + P_2^2 + 2y\sqrt{\frac{\omega_2}{\omega_1}}P_1 X_2) - \frac{N}{2}\omega_R. \tag{12}$$

Here, $\omega_1$ corresponds to $-\delta_c$ and $\omega_2$ equals $\omega_R$. In contrast to the original Dicke-model Hamiltonian explored in Ref. [33], which emphasized the coupling of coordinates with coordinates, Equation (12) showcases a coupling between coordinates and momenta (evident in the penultimate term of Equation (12)). This distinction necessitates a fresh approach in analyzing the Hamiltonian, distinct from the methodologies employed in Ref. [33].

In order to compute the QFI based on Equation (3) in relation to the normal phase, obtaining the density matrix of $p_n$ from Equation (3) in the energy basis is crucial. We achieve this by following a three-step process: (i) Firstly, we decouple the two harmonic oscillators in Hamiltonian (12) using Bogoliubov's transformations. The excitation energies $\varepsilon_k$ $(k = 1, 2)$ are determined as $\varepsilon_k^2 = (\omega_1^2 + \omega_2^2 + (-1)^{k-1}\sqrt{\left(\omega_1^2 - \omega_2^2\right)^2 + 4y^2\omega_1\omega_2})/2$. With this knowledge, we can plot the ground state energy and excitation energies, represented by solid black curves in Figure 2a and 2b, respectively. It is worth noting that the ground state energy remains continuous across the critical point, whereas the second derivative of the ground state energy diverges, serving as an indicator of the superradiant quantum phase transition. (ii) Secondly, we obtain the reduced density matrix of the atoms in spatial coordinates as follows:

$$\rho_X\left(X_2, X_2'\right) = \exp\left\{\frac{-\Omega_{ca}}{2\sinh\beta\Omega_{ca}}\left[\cosh(\beta\Omega_{ca})(X_2^2 + X_2'^2) - 2X_2X_2'\right]\right\}, \tag{13}$$

where $\Omega_{ca} = \frac{\varepsilon_2\varepsilon_3}{\varepsilon_3 c^2 + \varepsilon_2 s^2}\sqrt{1 + \frac{s^2c^2(\varepsilon_2-\varepsilon_3)^2}{\varepsilon_2\varepsilon_3}}$, $c = \cos\gamma$, $s = \sin\gamma$, $\tan 2\gamma = \frac{2y\sqrt{\omega_1\omega_2}}{\omega_1^2-\omega_2^2}$, and $\beta = (k_B T)^{-1}$. (iii) Finally, we derive the eigenvalues of the population $p_n$ corresponding to the energy eigenstate $|n\rangle$ in Equation (3) as $p_n = \exp(-n\beta\Omega_{ca})[1 - \exp(-\beta\Omega_{ca})]$.

Subsequently, one can calculate the squeezing parameter of the atoms, given by $\xi_R^2 = \frac{4\min\left(\Delta S_x^2, \Delta S_y^2\right)}{N}$. The detailed variances are expressed as:

$$\begin{aligned} \left(\Delta S_x\right)^2 &= \frac{N}{4}\frac{\omega_2}{\Omega_{ca}}\frac{e^{\beta\Omega_{ca}}+1}{e^{\beta\Omega_{ca}}-1}, \\ \left(\Delta S_y\right)^2 &= \frac{N}{4}\frac{\Omega_{ca}}{\omega_2}\frac{e^{\beta\Omega_{ca}}+1}{e^{\beta\Omega_{ca}}-1}. \end{aligned} \tag{14}$$

Consequently, the squeezing parameter is:

$$\xi_R^2 = \frac{4(\Delta S_y)^2}{N} = \frac{\Omega_{ca}}{\omega_2}\frac{e^{\beta\Omega_{ca}}+1}{e^{\beta\Omega_{ca}}-1}, \tag{15}$$

depicted by the solid black curves in Figure 1c. As anticipated, $\xi_R^2$ diverges at the critical point of the quantum phase transition.

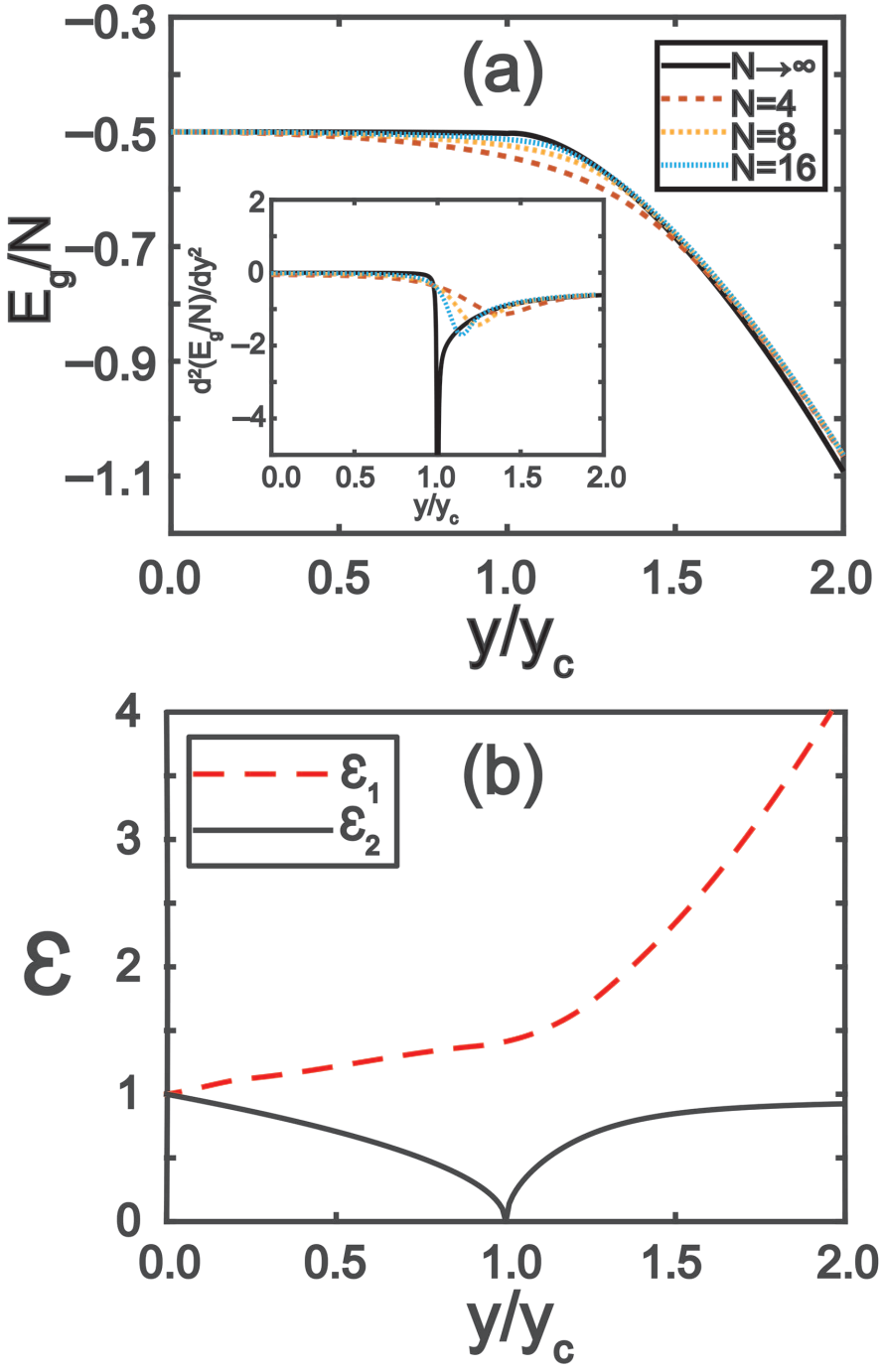


**Figure 2.** (**a**) Ground state energy of Hamiltonian (Equation (11)) and its second derivative of $d^2(E_g/N)/dy^2$ as a function of the coupling coefficient $y$. Solid lines: analytical results in the thermodynamic limit (i.e., $N = \infty$). Dashed lines: numerical results for a finite number of the atoms $N = 4, 8, 16$. (**b**) Eigenergies of the upper and lower polariton excitations on the Hamiltonian as a function of the coupling coefficient $y$ in the thermodynamic limit. Parameters are chosen as $\delta_c = -1\omega_R$ and $u = -0.1\omega_R$.

Now we are ready to calculate the QFI associated with the normal phase. If we choose $\hat{G}_1 = \hat{S}_x$ as the phase-shift generator, we can obtain the corresponding QFI as follows

$$F_1^{\mathrm{np}}(\rho, G_1) = N\frac{\omega_2}{\Omega_{ca}}\frac{e^{\beta\Omega_{ca}}-1}{e^{\beta\Omega_{ca}}+1}. \tag{16}$$

For a different choice $\hat{G}_2 = \hat{S}_y$, we can obtain the corresponding QFI $F_2(\rho, G_2) = N\frac{\Omega_{ca}}{\omega_2}\frac{e^{\beta\Omega_{ca}}-1}{e^{\beta\Omega_{ca}}+1}$. Obviously, it is better to choose $\hat{G}_1 = \hat{S}_x$ as the phase-shift generator due to $F_1 > F_2$, and the corresponding QFI is given by Equation (16), which has been plotted into the solid black curves in Figure 1a,b. As is expected, QFI is divergent across the critical point of the quantum phase transition.

We proceed to compute the Quantum Fisher Information (QFI) in the superradiant phase. In this phase, considering the population inversion that occurs across a multitude of atoms, one can decompose the operators $\hat{a}$ and $\hat{b}$ from Hamiltonian (11) as follows:

$$\hat{a} = \delta a \pm i\sqrt{N}\alpha_s \quad \text{and} \quad \hat{b} = \delta b \pm \sqrt{N}\beta_s. \tag{17}$$

Here, $\alpha_s$ and $\beta_s$ represent the mean-field components, while $\delta a$ and $\delta b$ denote the quantum fluctuations for each subsystem. For clarity, we will adopt the notation $a = \delta a + i\sqrt{N}\alpha_s$ and $b = \delta b + \sqrt{N}\beta_s$, noting that both choices of shifts yield consistent results. There exists a pair of real values for $\beta_s$ and $\alpha_s$ that eliminate the linear terms in the Hamiltonian (11) within the displaced phase space. These values are determined by:

$$\begin{cases} \alpha_s\left(\delta_c - {\beta_s}^2 u\right) = \beta_s\sqrt{1-\beta_s^2}y \\ \alpha_s^2\beta_s u + \beta_s\omega_R = \frac{\alpha_s\left(2\beta_s^2-1\right)y}{\sqrt{1-\beta_s^2}}. \end{cases} \tag{18}$$

The trivial solution, where $\alpha_s = \beta_s = 0$, corresponds to the normal phase. For the non-trivial case where $\alpha_s \neq 0$ and $\beta_s \neq 0$, a physically meaningful solution arises:

$$\beta_s^2 = \frac{\delta_c\left[1-\sqrt{1-\frac{u\left(y^2-y_c^2\right)}{\delta_c\left(y^2-\frac{uy_c^2}{\delta_c}\right)}}\right]}{u}. \tag{19}$$

This solution exists within the range $0 < \beta_s^2 \leq 1$ if and only if $y$ exceeds $y_c$, defined as $\sqrt{-\delta_C\omega_R}$. By approximating the Hamiltonian (11) to the second order and substituting Equation (19) into it, we obtain the effective Hamiltonian in the superradiant phase at finite temperature:

$$\begin{aligned} H_s =& M_0\delta a^\dagger\delta a + M_y\delta b^\dagger\delta b + \frac{M_x - M_y}{4}\left(\delta b^\dagger + \delta b\right)^2 \\ &+ \frac{i}{2}M_c\left(\delta a^\dagger - \delta a\right)\left(\delta b^\dagger + \delta b\right) + E_g, \end{aligned} \tag{20}$$

where the coefficients and ground state energy $E_g$ are defined as follows: $M_0 = -\delta_C + u\beta_s^2$, $M_x = \omega_R + u\alpha_s^2 - y\alpha_s\beta_s\frac{3-2\beta_s^2}{\left(1-\beta_s^2\right)^{3/2}}$, $M_y = \omega_R + u\alpha_s^2 - y\alpha_s\beta_s\frac{1}{\left(1-\beta_s^2\right)^{1/2}}$, $M_c = 2u\alpha_s\beta_s + y\frac{1-2\beta_s^2}{\left(1-\beta_s^2\right)^{1/2}}$, and

$$E_g = \alpha_s^2\beta_s^2 Nu - \alpha_s^2 N\delta_c + \beta_s^2 N\omega_R + 2\alpha_s\beta_s\sqrt{1-\beta_s^2}Ny - \omega_R j. \tag{21}$$

Utilizing Equation (21), we have plotted the ground state energy and its second derivative, depicted as solid black curves in Figure 2a. As shown in the inset of Figure 2a, the second derivative of the ground state energy diverges at the critical point of $y_c$, as expected.

Similar to the treatment in the normal phase, we typically introduce operators $\tilde{X}_{1,2} = 1/\sqrt{2\tilde{\omega}_{1,2}}(\delta a_{1,2}^\dagger + \delta a_{1,2})$ and $\tilde{P}_{1,2} = i\sqrt{\tilde{\omega}_{1,2}/2}(\delta a_{1,2}^\dagger - \delta a_{1,2})$, where $\tilde{\omega}_1 = M_0$ and $\tilde{\omega}_2 = M_y$. Then, by defining $\Omega_1 = \tilde{\omega}_1$ and $\Omega_2 = \sqrt{\tilde{\omega}_2^2 + (M_x - M_y)\tilde{\omega}_2}$, we rewrite Hamiltonian (20) as follows:

$$H_{s_1} = \frac{1}{2}\left[\Omega_1^2\tilde{X}_1^2 + \tilde{P}_1^2 + \Omega_2^2\tilde{X}_2^2 + \tilde{P}_2^2 + 2M_c\sqrt{\frac{\tilde{\omega}_2}{\tilde{\omega}_1}}\tilde{P}_1\tilde{X}_2\right]. \tag{22}$$

Equation (22) has the same structure as Equation (12) with the rescaled frequencies and coupling coefficient, $\Omega_1$, $\Omega_2$ and $M_c$. Therefore, by employing the same procedure used to derive $H_{np}$, we find the eigenvalues of the density operator as $p_n = \exp(-n\beta\Omega_{qa})[1 - \exp(-\beta\Omega_{qa})]$, where $\Omega_{qa} = \tilde{\varepsilon}_2\tilde{\varepsilon}_1\sqrt{1 + \tilde{s}^2\tilde{c}^2(\tilde{\varepsilon}_2 - \tilde{\varepsilon}_1)^2/\tilde{\varepsilon}_2\tilde{\varepsilon}_1}/(\tilde{\varepsilon}_1\tilde{c}^2 + \tilde{\varepsilon}_2\tilde{s}^2)$, $\tilde{c} = \cos\tilde{\gamma}$ and $\tilde{s} = \sin\tilde{\gamma}$ with $\tan 2\tilde{\gamma} = 2M_c\sqrt{\tilde{\omega}_1\tilde{\omega}_2}/(\Omega_1^2 - \Omega_2^2)$, $\tilde{\varepsilon}_1^2 = \frac{1}{2}(\Omega_1^2 + \Omega_2^2 + \sqrt{(\Omega_1^2 - \Omega_2^2)^2 + 4M_c^2\tilde{\omega}_1\tilde{\omega}_2})$ and $\tilde{\varepsilon}_2^2 = \frac{1}{2}(\Omega_1^2 + \Omega_2^2 - \sqrt{(\Omega_1^2 - \Omega_2^2)^2 + 4M_c^2\tilde{\omega}_1\tilde{\omega}_2})$. We proceed to calculate the analytical expression of the squeezing parameter in the superradiant phase at the finite temperature

$$\xi_{\tilde{R}}^2 = \frac{4\min\left(\Delta S_x^2, \Delta S_y^2\right)}{N} = \left(1 - \beta_s^2\right)\frac{\Omega_{qa}}{\tilde{\omega}_2}\frac{e^{\beta\Omega_{qa}} + 1}{e^{\beta\Omega_{qa}} - 1}, \tag{23}$$

which is routine to be plotted into Figure 1c. Again, the squeezing parameter is divergent as $y \to y_c$ as a signature of the superradiant quantum phase transition.

Lastly, we compute the Quantum Fisher Information (QFI) of atoms in the superradiant phase at finite temperature. Choosing $\hat{G}_1 = \hat{S}_x$ as the phase-shift generator yields the corresponding QFI:

$$F_I^{\mathrm{SP}} = N\frac{(1 - 2\beta_s^2)^2}{1 - \beta_s^2}\frac{\tilde{\omega}_2}{\Omega_{qa}}\frac{e^{\beta\Omega_{qa}} - 1}{e^{\beta\Omega_{qa}} + 1}. \tag{24}$$

In Figure 1a, the black solid curves represent the results obtained from Equations (16) and (24). Evidently, the QFI diverges at the critical point $y = y_c$, indicating a significant change in the quantum state of the system.

### *3.3. Probing Quantum Phase Transition of a Quantum-Gas Cavity QED by Quantum Fisher Information*

In Sections 3.1 and 3.2, we analytically derived the Quantum Fisher Information (QFI) for the Hamiltonian in Equation (1)—at zero temperature [Equations (7) and (10)] and finite temperature in the thermodynamic limit [Equations (16) and (24)]. In Section 3.3, we extend this to finite atom numbers by numerically computing QFI via Equation (3) and analyzing its use for detecting quantum phase transitions (QPTs) in quantum-gas cavity QED.

To compute QFI numerically, we first find the eigenvalues and eigenvectors of the density operator $\hat{\rho}$. Using the method of Ref. [33], we solve for the ground state $|g\rangle = \sum_{n=0}^{N}\sum_{m=-j}^{j} c_{n,m}$ of the finite-$N$ Hamiltonian (Equation (1)), where $N$ is the cutoff photon number. We minimize Equation (1) to obtain $c_{n,m}$, then trace out the bosonic field to get the atomic density operator: $\hat{\rho} = \mathrm{Tr}_F(|g\rangle\langle g|)$. With $\hat{\rho}$, we compute its eigenvalues/eigenvectors for $N \leq 20$ and substitute into Equation (3). We plot QFI (Figure 1a,b) and ground-state energy (Figure 2a) from these numerics.

Utilizing the data presented in Figures 1 and 2, we are poised to devise a methodology for detecting quantum phase transitions in the Hamiltonian of Equation (1)

through QFI. Let us highlight some key aspects of the quantum phase transition and QFI as defined in Equation (2). Firstly, the rescaled cavity photon number, denoted as $n_c = |\delta_c|/\omega_R\langle\hat{a}^\dagger\hat{a}\rangle$, serves as an order parameter. It vanishes for $y < y_c$ and becomes finite with $n_c = (y^4 - y_c^4)/4y$ for $y > y_c$. This order parameter directly reflects the symmetry breaking. Secondly, the rescaled ground state energy approaches a limit as $\lim_{y\to y_c} E_{\rm np} = \delta/4 = \lim_{y\to y_c} E_{\rm sp}$, indicating continuity at the critical point $y = y_c$, as illustrated in Figure 2a. However, the second derivative of the ground state energy exhibits a discontinuity, as evidenced by the inset curves of Figure 2a, revealing the second-order nature of the quantum phase transition. Thirdly, in proximity to the critical point, as demonstrated in Equations (7) and (10), the excitation energies in both the normal and superradiant phases tend to zero, proportional to $\propto |1 - y^2/y_c^2|^{1/2}$ as shown in Figure 2b. Consequently, the QFI in Equation (2) is expected to diverge as $\propto |y - y_c|^2$, which is corroborated by Equations (7) and (10).

Figure 1a is the heart of our QPT detection: it shows QFI for Equation (1) Hamiltonian. Solid red/black curves are thermodynamic-limit ($N, V \to \infty$, $N/V$ fixed) analytical QFI for zero/finite temperature; dashed curves are numerical QFI for finite $N$. As $N$ grows, numerical QFI converges to the thermodynamic limit—matching our analytics. Most critically, both approaches show QFI **diverging at $y = y_c$**—unambiguous proof of the superradiant quantum phase transition.

## 4. Discussion and Conclusions

The emphasis and purpose of this work is to design a protocol using QFI to characterize the symmetry-breaking quantum phase transition (QPT) of the Dicke model in cavity QED—specifically across its critical point—relying on experimentally accessible tools. Validating this physics requires experimentally implementing cavity QED, which hinges on tightly controlled light–matter interactions [1–4]. A prototypical setup uses a Bose–Einstein condensate (BEC) in an optical cavity, where effective atom-field coupling is tuned by varying pump laser intensity over time. Notably, while this cold-atom approach has unique benefits, our results extend to quantum well waveguide implementations, where light–matter interaction can be activated in less than a light cycle [36].

Our methodology to characterize the Dicke model's quantum phase transition (QPT) in cavity QED across the critical point leverages Quantum Fisher Information (QFI) measurements. Experimentally, QFI—at zero and finite temperatures—can be extracted via dynamic susceptibility measurements using Bragg spectroscopy, a technique established in cold-atom and condensed-matter systems [31]. Alternatively, QFI and its first derivative can be extracted by extrapolating polynomial fits to the squared Hellinger distance between probability distributions, as proposed in Ref. [32].

With these experimental pathways in place, the phenomena we study should be accessible with current capabilities. We restrict our analysis to the Schrieffer–Wolff transformation (valid for $|\delta_c|/(\omega_R N) \ll 1$ at zero temperature) and the Holstein–Primakoff approximation (thermodynamic limit, finite temperature). For regimes beyond these approximations, the functional path integral method is reliable but lies outside our scope [26].

In summary, we use the QFI to characterize the symmetry-breaking quantum phase transition in the cavity-QED Dicke model across the critical point. At zero temperature, we derive analytical QFI expressions for the limit where the atomic transition frequency (scaled by the cavity frequency) tends to infinity. We also analyze finite-temperature QFI effects in the thermodynamic limit and for large but finite atom numbers. Consistently, we find a QFI singularity as coupling crosses the critical point—a distinct signature of quantum criticality. This divergent QFI behavior correlates directly with dynamic susceptibility measurements via Bragg spectroscopy—an accessible experimental tool.

**Author Contributions:** Conceptualization, Z.L.; Investigation, L.Z.; Methodology, L.Z. and Z.L.; software, Q.W.; writing—original draft preparation, L.Z.; writing—review and editing, Z.L.; supervision, Z.L. All authors have read and agreed to the published version of the manuscript.

**Funding:** This work was supported by the National Natural Science Foundation of China (Grants No. 12574301) and the Zhejiang Provincial Natural Science Foundation (Grant No. LZ25A040004).

**Data Availability Statement:** Data are contained within the article.

**Acknowledgments:** We thank Guangri Jin and Ying Hu for stimulating discussions and helpful assistance, as well as Yanhong Xiao for her insightful guidance.

**Conflicts of Interest:** The authors declare no conflicts of interest.

## Appendix A. Derivation of the Effective Hamiltonian of Equation (1)

This Appendix A provides a detailed derivation of the effective Dicke-like Hamiltonian of Equation (1) of the main text starting from the full microscopic description. Consider a system of $N$ atoms in a Bose–Einstein condensate coupled to a single-mode optical cavity. The complete Hamiltonian is given by:

$$\hat{H} = -\Delta_c \hat{a}^\dagger \hat{a} + \int_{-L/2}^{L/2} \hat{\Psi}^\dagger(x) \left[ -\frac{\hbar^2}{2m}\frac{d^2}{dx^2} + \hbar U_0 \hat{a}^\dagger \hat{a} \cos^2 kx + i\eta_t \cos kx (\hat{a}^\dagger - \hat{a}) \right] \hat{\Psi}(x) dx, \quad \text{(A1)}$$

where all parameters maintain the same definitions as in the main text. We employ the two-mode momentum expansion:

$$\hat{\Psi}(x) = \frac{1}{\sqrt{L}} (\hat{c}_0 + \sqrt{2}\hat{c}_1 \cos kx). \quad \text{(A2)}$$

Substituting Equation (A2) into the Hamiltonian of Equation (A1) and evaluating term by term:

Kinetic Energy Term:

$$\int \hat{\Psi}^\dagger(x) \left( -\frac{\hbar^2}{2m}\frac{d^2}{dx^2} \right) \hat{\Psi}(x) dx = \frac{\hbar^2 k^2}{2m} \hat{c}_1^\dagger \hat{c}_1 \quad \text{(A3)}$$

Optical Lattice Term:

$$\int \hat{\Psi}^\dagger(x) \left( \hbar U_0 \hat{a}^\dagger \hat{a} \cos^2 kx \right) \hat{\Psi}(x) dx = \frac{1}{2}\hbar U_0 \hat{a}^\dagger \hat{a} (\hat{c}_0^\dagger \hat{c}_0 + \hat{c}_1^\dagger \hat{c}_1) + \frac{1}{4}\hbar U_0 \hat{a}^\dagger \hat{a} \hat{c}_1^\dagger \hat{c}_1 \quad \text{(A4)}$$

Pumping Term:

$$\int \hat{\Psi}^\dagger(x) \left[ i\eta_t \cos kx (\hat{a}^\dagger - \hat{a}) \right] \hat{\Psi}(x) dx = \frac{\sqrt{2}}{2} i\eta_t (\hat{c}_0^\dagger \hat{c}_1 + \hat{c}_1^\dagger \hat{c}_0)(\hat{a}^\dagger - \hat{a}) \quad \text{(A5)}$$

Combining all above three terms together, we obtain:

$$\hat{H} = -\Delta_c \hat{a}^\dagger \hat{a} + \frac{1}{2}\hbar U_0 N \hat{a}^\dagger \hat{a} + \frac{\hbar^2 k^2}{2m} \hat{c}_1^\dagger \hat{c}_1 + \frac{\sqrt{2}}{2} i\eta_t (\hat{c}_0^\dagger \hat{c}_1 + \hat{c}_1^\dagger \hat{c}_0)(\hat{a}^\dagger - \hat{a}) + \frac{1}{4}\hbar U_0 \hat{c}_1^\dagger \hat{c}_1 \hat{a}^\dagger \hat{a}. \quad \text{(A6)}$$

We proceed to introduce the Schwinger spin operators:

$$\hat{S}_x = \frac{1}{2}(\hat{c}_1^\dagger \hat{c}_0 + \hat{c}_0^\dagger \hat{c}_1), \qquad \hat{S}_z = \frac{1}{2}(\hat{c}_1^\dagger \hat{c}_1 - \hat{c}_0^\dagger \hat{c}_0). \quad \text{(A7)}$$

Utilizing the relations $\hat{c}_1^\dagger \hat{c}_1 = \hat{S}_z + N/2$ and $\hat{c}_0^\dagger \hat{c}_0 = N/2 - \hat{S}_z$, we rewrite the Hamiltonian of Equation (A6)

$$\hat{H} = -\Delta_c \hat{a}^\dagger \hat{a} + \frac{1}{2}\hbar U_0 N \hat{a}^\dagger \hat{a} + \frac{\hbar^2 k^2}{2m}\left(\hat{S}_z + \frac{N}{2}\right) + i\eta_t \sqrt{2}\hat{S}_x(\hat{a}^\dagger - \hat{a}) + \frac{1}{4}\hbar U_0\left(\hat{S}_z + \frac{N}{2}\right)\hat{a}^\dagger \hat{a} \quad \text{(A8)}$$

After rearranging terms and setting $\hbar = 1$, we arrive at the final form:

$$\hat{H} = \omega_R \hat{S}_z - \delta_c \hat{a}^\dagger \hat{a} + \frac{iy}{\sqrt{N}}(\hat{a}^\dagger - \hat{a})\hat{S}_x + \frac{u}{2}\hat{a}^\dagger \hat{a}\left(1 + \frac{2\hat{S}_z}{N}\right) \quad \text{(A9)}$$

where the parameters are defined as: $\omega_R = \frac{\hbar^2 k^2}{2m}$, $y = \sqrt{2N}\eta_t$, $u = \frac{NU_0}{4}$, and $\delta_c = \Delta_c - 2u$. This Hamiltonian of Equation (A9) corresponds to the Dicke-like model of Equation (1) presented in the main text.

## Appendix B. Effective Low-Energy Hamiltonian of Equation (5) in the Normal Phase

This Appendix B provides a detailed derivation of effective low-energy Hamiltonian of Equation (5) of the main text. To derive the effective low-energy Hamiltonian in the normal phase ($y \leq y_c$), we apply the Schrieffer–Wolff transformation $\hat{U} = \exp\left[\frac{y}{(\omega_R\sqrt{N})}(a - a^\dagger)\hat{S}_y\right]$ to the full Hamiltonian in Equation (A9):

$$\begin{aligned}
\hat{U}^\dagger \hat{H} \hat{U} = {} & \omega_R\left[\cos\left(i\frac{y(\hat{a}^\dagger - \hat{a})}{\omega_R\sqrt{N}}\right)\hat{S}_z - \sin\left(i\frac{y(\hat{a}^\dagger - \hat{a})}{\omega_R\sqrt{N}}\right)\hat{S}_x\right] \\
& - \delta_c\left(\hat{a}^\dagger - \frac{\hat{S}_y}{\omega_R\sqrt{N}}y\right)\left(\hat{a} - \frac{\hat{S}_y}{\omega_R\sqrt{N}}y\right) \\
& + \frac{iy}{\sqrt{N}}\left(\hat{a}^\dagger - \hat{a}\right)\left[\cosh\left(\frac{y(\hat{a}^\dagger - \hat{a})}{\omega_R\sqrt{N}}\right)\hat{S}_x + i\sinh\left(\frac{y(\hat{a}^\dagger - \hat{a})}{\omega_R\sqrt{N}}\right)\hat{S}_z\right] \\
& + u\left(\hat{a}^\dagger - \frac{\hat{S}_y}{\omega_R\sqrt{N}}y\right)\left(\hat{a} - \frac{\hat{S}_y}{\omega_R\sqrt{N}}y\right) \\
& \times\left(\frac{1}{2} + \frac{1}{N}\left[\cosh\left(\frac{y(\hat{a}^\dagger - \hat{a})}{\omega_R\sqrt{N}}\right)\hat{S}_z - i\sinh\left(\frac{y(\hat{a}^\dagger - \hat{a})}{\omega_R\sqrt{N}}\right)\hat{S}_x\right]\right) \quad \text{(A10)}
\end{aligned}$$

Using Taylor expansions for the hyperbolic functions:

$$\sinh x = \frac{e^x - e^{-x}}{2} = \sum_{n=0}^{\infty}\frac{x^{2n+1}}{(2n+1)!}, \quad x \in (-\infty, +\infty) \quad \text{(A11)}$$

$$\cosh x = \frac{e^x + e^{-x}}{2} = \sum_{n=0}^{\infty}\frac{x^{2n}}{(2n)!}, \quad x \in (-\infty, +\infty) \quad \text{(A12)}$$

and keeping terms up to second order in the small parameter $\frac{y}{\omega_R\sqrt{N}}$, we obtain:

$$\begin{aligned}
\hat{U}^\dagger \hat{H} \hat{U} \approx {} & -\delta_c \hat{a}^\dagger a + \omega_R\left[\left(1 + \frac{1}{2}\left(\frac{y^2}{\omega_R^2 N}\left(\hat{a}^\dagger - \hat{a}\right)^2\right)\right)\hat{S}_z - i\frac{y}{\omega_R\sqrt{N}}\left(\hat{a}^\dagger - \hat{a}\right)\hat{S}_x\right] \\
& + \frac{iy}{\sqrt{N}}\left(\hat{a}^\dagger - \hat{a}\right)\left[\hat{S}_x + i\frac{y}{\omega_R\sqrt{N}}\left(\hat{a}^\dagger - \hat{a}\right)\hat{S}_z\right] + u\hat{a}^\dagger \hat{a}\left(\frac{1}{2} + \frac{\hat{S}_z}{N}\right) \\
= {} & -\delta_c \hat{a}^\dagger a + \omega_R \hat{S}_z - \frac{y^2}{2\omega_R N}\left(\hat{a}^\dagger - \hat{a}\right)^2 \hat{S}_z + u\hat{a}^\dagger \hat{a}\left(\frac{1}{2} + \frac{\hat{S}_z}{N}\right) \quad \text{(A13)}
\end{aligned}$$

Under the conditions $\frac{|\delta_c|}{\omega_R N} \ll 1$ and $|u| < |\delta_c|$, and neglecting terms proportional to $\sqrt{\frac{-\delta_c}{\omega_R N}}$, we take the expectation value in the spin-down state $|\downarrow\rangle$ to obtain the effective low-energy Hamiltonian for the normal phase:

$$H_{\rm np} = \langle\downarrow|\hat{U}^\dagger \hat{H} \hat{U}|\downarrow\rangle = -\delta_c \hat{a}^\dagger a + \frac{y^2}{4\omega_R}(\hat{a}^\dagger - \hat{a})^2 - \frac{N\omega_R}{2}. \tag{A14}$$

Equation (A14) is the effective Hamiltonian of Equation (5) used in the main text for analyzing the normal phase of the system. We remark that the last term of $u\hat{a}^\dagger\hat{a}\left(\frac{1}{2} + \frac{\hat{S}_z}{N}\right)$ in Hamiltonian (1) plays no role when we derive Equation (A14) because of $\langle\downarrow|\left(\frac{1}{2} + \frac{\hat{S}_z}{N}\right)|\downarrow\rangle = 0$.

## Appendix C. Effective Hamiltonian of Equation (8)

This Appendix C provides a detailed derivation of effective Low-Energy Hamiltonian of Equation (8) of the main text. Before proceeding, we want to remark the effect of the last term of $u\hat{a}^\dagger\hat{a}\left(\frac{1}{2} + \frac{\hat{S}_z}{N}\right)$ in Hamiltonian (1). As shown in the Appendix B, this term is equal to zero when we derive Equation (A14). It is supposed that the term $u\hat{a}^\dagger\hat{a}\left(\frac{1}{2} + \frac{\hat{S}_z}{N}\right)$ can still be neglected when we consider the super-radiance phase because its effect is renormalized the frequency of the term of $a^\dagger a$ into $\delta_c \to \delta_c - u\left(\frac{1}{2} + \frac{\bar{S}_z}{N}\right)$. Considering that the super-radiance phase mainly is driven by the $y$-term in Hamiltonian of Equation (1), we will ignore the last term of Equation (1) for the sake of simplifying the calculation.

For the superradiant phase, the original Hamiltonian Equation (A9) can be reasonably rewritten into

$$\hat{H} = -\delta_c \hat{a}^\dagger \hat{a} + \omega_R \hat{S}_z + \frac{iy}{\sqrt{N}}\left(\hat{a}^\dagger - \hat{a}\right)\hat{S}_x$$

Next, we apply the displacement transformation to the Hamiltonian Equation (A9) by introducing the displacement operator $D(\alpha)$ with $\alpha^* - \alpha = -i\beta$:

$$\begin{aligned} D^\dagger(\alpha) H D(\alpha) &= -\delta_c\left(\hat{a}^\dagger + \alpha^*\right)(\hat{a} + \alpha) + \omega_R \hat{S}_z \\ &+ \frac{iy}{\sqrt{N}}\left(\hat{a}^\dagger - \hat{a} + \alpha^* - \alpha\right)\hat{S}_x. \end{aligned} \tag{A15}$$

Substituting $\alpha^* - \alpha = -i\beta$ into above Equation (A15) and defining $\frac{y\beta}{\omega_R\sqrt{N}} = \tan 2\theta$ and $\cos 2\theta \hat{S}_z + \sin 2\theta \hat{S}_x = e^{-i2\hat{S}_y\theta}\hat{S}_z e^{i2\hat{S}_y\theta}$, we obtain

$$\begin{aligned} D^\dagger(\alpha) H D(\alpha) &= -\delta_c \hat{a}^\dagger \hat{a} + \omega_R\left(\hat{S}_z + \frac{y\beta}{\omega_R\sqrt{N}}\hat{S}_x\right) + \frac{iy}{\sqrt{N}}\left(\hat{a}^\dagger - \hat{a}\right)\hat{S}_x \\ &- \delta_c\left(\hat{a}^\dagger\alpha + \alpha^*\hat{a}\right) - \delta_c|\alpha|^2 \\ &= -\delta_c \hat{a}^\dagger \hat{a} + \omega_R\left(\hat{S}_z + \tan 2\theta \hat{S}_x\right) + \frac{iy}{\sqrt{N}}\left(\hat{a}^\dagger - \hat{a}\right)\hat{S}_x \\ &- \delta_c\left(\hat{a}^\dagger\alpha + \alpha^*\hat{a}\right) - \delta_c|\alpha|^2 \\ &= -\delta_c \hat{a}^\dagger \hat{a} + \frac{\omega_R}{\cos 2\theta}\left(\cos 2\theta \hat{S}_z + \sin 2\theta \hat{S}_x\right) + \frac{iy}{\sqrt{N}}\left(\hat{a}^\dagger - \hat{a}\right)\hat{S}_x \\ &- \delta_c\left(\hat{a}^\dagger\alpha + \alpha^*\hat{a}\right) - \delta_c|\alpha|^2 \\ &= -\delta_c \hat{a}^\dagger \hat{a} + \frac{\omega_R}{\cos 2\theta} e^{-i2\hat{S}_y\theta}\hat{S}_z e^{i2\hat{S}_y\theta} + \frac{iy}{\sqrt{N}}\left(\hat{a}^\dagger - \hat{a}\right)\hat{S}_x \\ &- \delta_c\left(\hat{a}^\dagger\alpha + \alpha^*\hat{a}\right) - \delta_c|\alpha|^2. \end{aligned} \tag{A16}$$

Applying the rotation transformation $U^\dagger = e^{i2\hat{S}_y\theta}$ to $D^\dagger(\alpha)HD(\alpha)$ into Equation (A16), we proceed to obtain

$$\begin{aligned} U^\dagger D^\dagger(\alpha)HD(\alpha)U &= -\delta_c\hat{a}^\dagger\hat{a} + \frac{\omega_R}{\cos 2\theta}\hat{S}_z + \frac{iy}{\sqrt{N}}\left(\hat{a}^\dagger - \hat{a}\right)U^\dagger\hat{S}_x U \\ &- \delta_c\left(\hat{a}^\dagger\alpha + \alpha^*\hat{a}\right) - \delta_c|\alpha|^2. \end{aligned} \tag{A17}$$

Using $U^\dagger\hat{S}_x U = \cos 2\theta\hat{S}_x + \sin 2\theta\hat{S}_z$, we can simplify Equation (A17) further as follow

$$\begin{aligned} U^\dagger D^\dagger(\alpha)HD(\alpha)U =& -\delta_c\hat{a}^\dagger\hat{a} + \frac{\omega_R}{\cos 2\theta}\hat{S}_z \\ &+ \frac{iy}{\sqrt{N}}\left(\hat{a}^\dagger - \hat{a}\right)\left(\cos 2\theta\hat{S}_x + \sin 2\theta\hat{S}_z\right) \\ &- \delta_c\left(\hat{a}^\dagger\alpha + \alpha^*\hat{a}\right) - \delta_c|\alpha|^2 \\ =& -\delta_c\hat{a}^\dagger\hat{a} + \frac{\omega_R}{\cos 2\theta}\hat{S}_z \\ &+ \frac{iy}{\sqrt{N}}\left(\hat{a}^\dagger - \hat{a}\right)\cos 2\theta\hat{S}_x + \frac{iy}{\sqrt{N}}\left(\hat{a}^\dagger - \hat{a}\right)\sin 2\theta\hat{S}_z \\ &- \delta_c\left(\hat{a}^\dagger\alpha + \alpha^*\hat{a}\right) - \delta_c|\alpha|^2 \end{aligned}$$

Assuming $\alpha$ is purely imaginary, $\alpha^* - \alpha = -i\beta = -2\alpha$ i.e., $\beta = -2i\alpha$, then we have:

$$\begin{aligned} H_{\text{sp}} =& U^\dagger D^\dagger(\alpha)HD(\alpha)U \\ =& -\delta_c\hat{a}^\dagger\hat{a} + \frac{\omega_R}{\cos 2\theta}\hat{S}_z + \frac{iy}{\sqrt{N}}\left(\hat{a}^\dagger - \hat{a}\right)\cos 2\theta\hat{S}_x \\ &+ \left(\frac{iy}{\sqrt{N}}\sin 2\theta\hat{S}_z - \delta_c\alpha\right)\left(\hat{a}^\dagger - \hat{a}\right) - \delta_c|\alpha|^2 \\ \approx& -\delta_c\hat{a}^\dagger\hat{a} + \frac{\omega_R}{\cos 2\theta}\hat{S}_z + \frac{iy}{\sqrt{N}}\left(\hat{a}^\dagger - \hat{a}\right)\cos 2\theta\hat{S}_x \\ &+ \left(\frac{iy\sqrt{N}}{2}\sin 2\theta - \delta_c\alpha\right)\left(\hat{a}^\dagger - \hat{a}\right) - \delta_c|\alpha|^2 \end{aligned}$$

where we approximate $\frac{iy}{\sqrt{N}}\sin 2\theta\hat{S}_z - \delta_c\alpha$ by taking $\hat{S}_z \to N/2$, i.e., $\frac{iy}{\sqrt{N}}\sin 2\theta\hat{S}_z - \delta_c\alpha \to \frac{iy\sqrt{N}}{2}\sin 2\theta - \delta_c\alpha$.

To eliminate the linear term in the above expression, $\alpha$ must satisfy $\delta_c\alpha = i\frac{y}{2}\sqrt{N}\sin 2\theta$. Using $\frac{y\beta}{\omega_R\sqrt{N}} = \tan 2\theta$ and $\sin 2\theta = \frac{\tan 2\theta}{\sqrt{1+\tan^2 2\theta}}$. In such we obtain

$$\alpha^2 = \frac{\omega_R^2 N}{4y^2} - \frac{y^2 N}{4\delta_c^2}$$

Introducing $y_c = \sqrt{-\delta_c\omega_R}$, the expression of $\alpha^2$ can be deduced into

$$\begin{aligned} \alpha^2 =& \frac{\omega_R^2 N}{4y^2} - \frac{y^2 N}{4\delta_c^2} \\ =& -\frac{\omega_R N(-\omega_R\delta_c)}{4y^2\delta_c} + \frac{\omega_R y^2 N}{4\delta_c(-\omega_R\delta_c)} \\ =& -\frac{N}{4}\frac{\omega_R}{-\delta_c\left(\frac{y}{y_c}\right)^2}\left(\left(\frac{y}{y_c}\right)^4 - 1\right) \end{aligned}$$

Therefore, we have

$$\alpha = \pm i \sqrt{\frac{N}{4} \frac{\omega_R}{-\delta_c \left(\frac{y}{y_c}\right)^2}} \sqrt{\left(\frac{y}{y_c}\right)^4 - 1}$$

When $\alpha$ takes the above value, i.e., the linear term vanishes, defining $\tilde{\omega}_R = \frac{\omega_R}{\cos 2\theta} = \sqrt{\omega_R^2 - 4y^2\alpha^2/N}$ and $\tilde{y} = y\omega_R\sqrt{N}/\sqrt{\omega_R^2 N - 4y^2\alpha^2}$, we finally obtain

$$\tilde{H}_{\mathrm{sp}} = -\delta_c \hat{a}^\dagger \hat{a} + \tilde{\omega}_R \hat{S}_z + \frac{i\tilde{y}}{\sqrt{N}} \left(\hat{a}^\dagger - \hat{a}\right) \hat{S}_x - \delta_c |\alpha|^2. \tag{A18}$$

Equation (A18) is the effective Hamiltonian of Equation (8) used in the main text for analyzing the normal phase of the system.

## References


1. Hammerer, K.; Sørensen, A.S.; Polzik, E.S. Quantum interface between light and atomic ensembles. *Rev. Mod. Phys.* **2010**, *82*, 1041. [CrossRef]
2. Forn-Díaz, P.; Lamata, L.; Rico, E.; Kono, J.; Solano, E. Ultrastrong coupling regimes of light-matter interaction. *Rev. Mod. Phys.* **2019**, *91*, 025005. [CrossRef]
3. Frisk Kockum, A.; Miranowicz, A.; De Liberato, S.; Savasta, S.; Nori, F. Ultrastrong coupling between light and matter. *Nat. Rev. Phys.* **2019**, *1*, 19. [CrossRef]
4. Liu, J.; Liu, M.; Ying, Z.J.; Luo, H.G. Fundamental Models in the Light–Matter Interaction: Quantum Phase Transitions and the Polaron Picture. *Adv. Quantum Technol.* **2021**, *4*, 2000139. [CrossRef]
5. Ritsch, H.; Domokos, P.; Brennecke, F.; Esslinger, T. Cold atoms in cavity-generated dynamical optical potentials. *Rev. Mod. Phys.* **2013**, *85*, 553. [CrossRef]
6. Mivehvar, F.; Piazza, F.; Donner, T.; Ritsch, H. Cavity QED with quantum gases: New paradigms in many-body physics. *Adv. Phys.* **2021**, *70*, 1. [CrossRef]
7. Braak, D. Integrability of the Rabi model. *Phys. Rev. Lett.* **2011**, *107*, 100401. [CrossRef]
8. Pezzè, L.; Smerzi, A.; Oberthaler, M.K.; Schmied, R.; Treutlein, P. Quantum metrology with nonclassical states of atomic ensembles. *Rev. Mod. Phys.* **2018**, *90*, 035005. [CrossRef]
9. Polino, E.; Valeri, M.; Spagnolo, N.; Sciarrino, F. Photonic quantum metrology. *AVS Quantum Sci.* **2020**, *2*, 024703. [CrossRef]
10. Gross, C.; Bloch, I. Quantum simulations with ultracold atoms in optical lattices. *Science* **2017**, *357*, 995. [CrossRef]
11. Dimer, F.; Estienne, B.; Parkins, A.S.; Carmichael, H.J. Proposed realization of the Dicke-model quantum phase transition in an optical cavity QED system. *Phys. Rev. A* **2007**, *75*, 013804. [CrossRef]
12. Baumann, K.; Guerlin, C.; Brennecke, F.; Esslinger, T. Dicke quantum phase transition with a superfluid gas in an optical cavity. *Nature* **2010**, *464*, 1301. [CrossRef] [PubMed]
13. Ashhab, S. Superradiance transition in a system with a single qubit and a single oscillator. *Phys. Rev. A—At. Mol. Opt. Phys.* **2013**, *87*, 013826. [CrossRef]
14. Nagy, D.; Kónya, G.; Szirmai, G.; Domokos, P. Dicke-Model Phase Transition in the Quantum Motion of a Bose–Einstein Condensate in an Optical Cavity. *Phys. Rev. Lett.* **2010**, *104*, 130401. [CrossRef]
15. Lambert, N.; Emary, C.; Brandes, T. Entanglement and the Phase Transition in Single-Mode Superradiance. *Phys. Rev. Lett.* **2004**, *92*, 073602. [CrossRef] [PubMed]
16. Emary, C.; Brandes, T. Quantum Chaos Triggered by Precursors of a Quantum Phase Transition: The Dicke Model. *Phys. Rev. Lett.* **2003**, *90*, 044101. [CrossRef]
17. Emary, C.; Brandes, T. Chaos and the quantum phase transition in the Dicke model. *Phys. Rev. E* **2003**, *67*, 066203. [CrossRef]
18. Baumann, K.; Mottl, R.; Brennecke, F.; Esslinger, T. Exploring Symmetry Breaking at the Dicke Quantum Phase Transition. *Phys. Rev. Lett.* **2011**, *107*, 140402. [CrossRef]
19. Baden, M.P.; Arnold, K.J.; Grimsmo, A.L.; Parkins, S.; Barrett, M.D. Realization of the Dicke Model Using Cavity-Assisted Raman Transitions. *Phys. Rev. Lett.* **2014**, *113*, 020408. [CrossRef]
20. Kongkhambut, P.; Keßler, H.; Skulte, J.; Mathey, L.; Cosme, J.G.; Hemmerich, A. Realization of a Periodically Driven Open Three-Level Dicke Model. *Phys. Rev. Lett.* **2021**, *127*, 253601. [CrossRef]
21. Skulte, J.; Kongkhambut, P.; Rao, S.; Mathey, L.; Keßler, H.; Hemmerich, A.; Cosme, J.G. Condensate Formation in a Dark State of a Driven Atom-Cavity System. *Phys. Rev. Lett.* **2023**, *130*, 163603. [CrossRef]

22. Müller, K.; Strunz, W.T. Genuine Quantum Effects in Dicke-Type Models at Large Atom Numbers. *Phys. Rev. Lett.* **2025**, *135*, 123602. [CrossRef]
23. Larson, J.; Irish, E.K. Some remarks on 'superradiant' phase transitions in light-matter systems. *J. Phys. A Math. Theor.* **2017**, *50*, 174002. [CrossRef]
24. Dicke, R.H. Coherence in Spontaneous Radiation Processes. *Phys. Rev.* **1954**, *93*, 99. [CrossRef]
25. Hepp, K.; Lieb, E.H. On the superradiant phase transition for molecules in a quantized radiation field: The dicke maser model. *Ann. Phys.* **1973**, *76*, 360. [CrossRef]
26. Wang, Y.K.; Hioe, F.T. Phase Transition in the Dicke Model of Superradiance. *Phys. Rev. A* **1973**, *7*, 831. [CrossRef]
27. Braunstein, S.L.; Caves, C.M. Statistical distance and the geometry of quantum states. *Phys. Rev. Lett.* **1994**, *72*, 3439. [CrossRef] [PubMed]
28. Pezzé, L.; Smerzi, A. Entanglement, Nonlinear Dynamics, and the Heisenberg Limit. *Phys. Rev. Lett.* **2009**, *102*, 100401. [CrossRef]
29. Genoni, M.G.; Olivares, S.; Paris, M.G.A. Optical Phase Estimation in the Presence of Phase Diffusion. *Phys. Rev. Lett.* **2011**, *106*, 153603. [CrossRef] [PubMed]
30. Ma, J.; Huang, Y.X.; Wang, X.; Sun, C.P. Quantum Fisher information of the Greenberger-Horne-Zeilinger state in decoherence channels. *Phys. Rev. A* **2011**, *84*, 022302. [CrossRef]
31. Hauke, P.; Heyl, M.; Tagliacozzo, L.; Zoller, P. Measuring multipartite entanglement through dynamic susceptibilities. *Nat. Phys.* **2016**, *12*, 778. [CrossRef]
32. Strobel, H.; Muessel, W.; Linnemann, D.; Zibold, T.; Hume, D.B.; Pezzè, L.; Smerzi, A.; Oberthaler, M.K. Fisher information and entanglement of non-Gaussian spin states. *Science* **2014**, *345*, 424. [CrossRef] [PubMed]
33. Wang, T.L.; Wu, L.N.; Yang, W.; Jin, G.R.; Lambert, N.; Nori, F. Quantum Fisher information as a signature of the superradiant quantum phase transition. *New J. Phys.* **2014**, *16*, 063039. [CrossRef]
34. Tang, S.B.; Qin, H.; Liu, B.B.; Wang, D.Y.; Cui, K.; Su, S.L.; Yan, L.L.; Chen, G. Enhancement of quantum sensing in a cavity-optomechanical system around the quantum critical point. *Phys. Rev. A* **2023**, *108*, 053514. [CrossRef]
35. Hwang, M.J.; Puebla, R.; Plenio, M.B. Quantum Phase Transition and Universal Dynamics in the Rabi Model. *Phys. Rev. Lett.* **2015**, *115*, 180404. [CrossRef]
36. Günter, G.; Anappara, A.A.; Hees, J.; Sell, A.; Biasiol, G.; Sorba, L.; De Liberato, S.; Ciuti, C.; Tredicucci, A.; Leitenstorfer, A.; et al. Sub-cycle switch-on of ultrastrong light–matter interaction. *Nature* **2009**, *458*, 178. [CrossRef] [PubMed]